frontiers | Frontiers in Marine Science

TYPE Original Research
PUBLISHED 08 December 2022
DOI 10.3389/fmars.2022.1092343

OPEN ACCESS

EDITED BY
Leonel Pereira,
University of Coimbra, Portugal

REVIEWED BY
Meivelu Moovendhan,
Sathyabama Institute of Science and Technology, India
Osama M. Darwesh,
National Research Centre, Egypt

*CORRESPONDENCE
Hussein Elsayed Touliabah
hehassan@kau.edu.sa

SPECIALTY SECTION
This article was submitted to Marine Biotechnology and Bioproducts, a section of the journal Frontiers in Marine Science

RECEIVED 07 November 2022
ACCEPTED 22 November 2022
PUBLISHED 08 December 2022

CITATION
Touliabah HE, El-Sheekh MM and Makhlof MEM (2022) Evaluation of *Polycladia myrica* mediated selenium nanoparticles (PoSeNPS) cytotoxicity against PC-3 cells and antiviral activity against HAV HM175 (Hepatitis A), HSV-2 (Herpes simplex II), and Adenovirus strain 2.
Front. Mar. Sci. 9:1092343.
doi: 10.3389/fmars.2022.1092343

Evaluation of *Polycladia myrica* mediated selenium nanoparticles (PoSeNPS) cytotoxicity against PC-3 cells and antiviral activity against HAV HM175 (Hepatitis A), HSV-2 (Herpes simplex II), and Adenovirus strain 2

Hussein Elsayed Touliabah[1]*, Mostafa Mohamed El-Sheekh[2] and Mofida Elsayed Mohmed Makhlof[3]

[1]Biological Sciences Department, Faculty of Science and Arts, King Abdulaziz University, Rabigh, Saudi Arabia, [2]Botany Department, Faculty of Science, Tanta University, Tanta, Egypt, [3]Botany and Microbiology Department, Faculty of Science, Damanhour University, Damanhour, Egypt

Introduction: The trace element selenium is an essential micronutrient for the health of humans, animals, and microbesMany researchers have recently become interested in selenium nanoparticles (SeNPs) because of their biocompatibility, bioavailability, and low toxicity. Consequently, selenium nanoparticles are widely used in various biomedical applications and wastewater bioremediation due to their greater bioactivity. Green biosynthesis of nanoparticles is common and preferable nowadays.

Methods: In this work, the selenium nanoparticles were synthesized using the brown seaweed Polycladia myrica aqueous extract and characterized using seven parameters, SEM, TEM, UV spectra, Zeta potential, EDX, X-ray differaction and FTIR, then examined for their cytotoxicity using PC-3 cells and normal mammalian cells from the African green monkey kidney (Vero) were used to test the effectiveness of the produced Polycladia myrica mediated selenium nanoparticles as an anticancer agent and antiviral activity against HAV HM175 (Hepatitis A), HSV-2 (Herpes simplex II), and Adenovirus strain 2.

Results: The phycosynthesized nanoparticles exhibit antiviral activity (40.25 $\pm$ 2.61, 8.64 $\pm$ 0.82, and 17.39 $\pm$ 1.45%) against HAV-10, Adenovirus, and HSV-2, respectively. The IC50 values of the two cell types human prostate PC-3 and Vero were 123.51 $\pm$ 4.07 g/mL and 220.53 $\pm$ 6.89 g/ mL, respectively. The maximum inhibitory percent was 86.15 $\pm$ 2.31 against PC-3 cells. At the same time, at a concentration of 125 g/mL.

Disscusion: This work showed that PoSeNPS have good antiviral activity against HAV-10 virus with an antiviral percent of 40.25%, despite weak antiviral activity against Adenovirus and HSV-2 with antiviral percent (8.64% and 17.39%), respectively. The cytotoxicity effect of these nanoparticles was determined against PC-3 with a maximum inhibitory percent of 80.53%. These nanoparticles have no hazardous effect against normal Vero cells as the viability percent was (78.39% and 49.23%) for Vero cells and PC-3 cells, respectively, at 125 µg/mL.

KEYWORDS

Polycladia myrica, selenium nanoparticles, PC-3, antiviral, HAV HM175 (Hepatitis A), HSV-2 (Herpes simplex II), Adenovirus strain 2, PoSeNPS

1 Introduction

The use of material nanoparticles (NPs) with dimensions ranging from 1 to 100 nm and for a variety of applications that are distinct from those of the same materials' bigger particles has attracted significant attention to nanotechnology in recent decades in a variety of scientific fields (Gunalan et al., 2012; Bhuyar et al., 2020). The trace element selenium is an essential micronutrient for the health of humans, animals, and microbes. It is also a food supplement and is thought to have cancer-prevention properties. Through selenoproteins, antioxidant defense, cell signal transmission, immunological modulation, and other metabolic activities, selenium is an essential trace mineral for preserving human health (Labunskyy et al., 2014). According to earlier research, a selenium deficit is directly linked to high cancer, infectious disease, and cardiovascular disease mortality rates (Rayman, 2012; Hatfield et al., 2014; Liu et al., 2017).

Many researchers have recently become interested in selenium nanoparticles (SeNPs) because of their biocompatibility, bioavailability, and low toxicity. Consequently, selenium nanoparticles are widely used in various biomedical applications and wastewater bioremediation due to their greater bioactivity (El-Shanshoury et al., 2020; Bisht et al., 2022). In general, physical, chemical, and biological techniques can be used to create selenium nanoparticles. However, biologically produced SeNPs are preferred for medicinal purposes because this technique is more compatible with human organs and tissues. Numerous researchers have investigated how their uses in biological systems are affected by their size, shape, and technique of manufacture (Kulkarni and Muddapur, 2014; Bisht et al., 2022). Kong (Kong et al., 2011) found that Selenium nanoparticles have been discovered to be safer than other Selenium compounds, including monomethylated Selenium, sodium selenite, and selenomethionine, its anticancer activity and intrinsic mechanisms remain unknown.

Due to their distinctive biological and physicochemical features, green nanomaterials have greatly developed in various relevant study fields over the past few decades (Khalifa et al., 2019). Depending on their intended uses and applications, nanoparticles could be created by various precursors. However, inorganic functional platforms are extremely important for concurrent diagnostics, antidote administration, and therapy (Alaqad and Saleh, 2016; Alshalalfeh et al., 2016). The manufacture of nanoparticles by chemical methods was seen to have some drawbacks, including a high energy requirement, toxic chemicals, high prices, and the generation of hazardous byproducts. This necessitates the creation of new biological eco-friendly effective approaches that rely on reducing agents from natural resources (Sharma et al., 2015). Using living organisms' methods has some benefits, including being economical, easily accessible, non-toxic, and environmentally benign. Biomolecules were used in place of the conventional stabilizing and reducing agents (Ovais et al., 2018). Utilizing plants, animals, foods, agricultural waste, and microbes, as well as their various natural components to act as reducing, stabilizing, and capping agents, allow for the formation of physicochemical adsorption coating processes without the use of chemical reactions (Anwar et al., 2016; Arshad et al., 2017; Vincy et al., 2017; Anwar et al., 2021). Whether alive or dried, algae are an essential resource for producing nanoparticles. They come from various organic compounds that operate like a powerful agent for reducing target metals. "Bionanofactories" could be referred to algae (Arya et al., 2018). Due to the many valuable biological compounds that can create different nanoparticle patterns, algal species have been identified as an effective tool for nanoparticle creation. The biogenic production of nanoparticles using microalgae is a natural, safe, economical, ecologically responsible, non-toxic, low-temperature, and energy-efficient method used for various applications (Sharma et al., 2014). El-Sheekh et al., (2022) (used two blue-green algal strains; *Oscillatoria* sp. and *Spirulina platensis* for green synthesizing

of Ag_2O|AgO-NPs and Au-NPs, respectively. Compared to other animals, algae are crucial for manufacturing nanoparticles (yeast, bacteria, and fungi) (Sharma et al., 2014; Rauwel et al., 2015; El-Sheekh and El-Kassas, 2016).

One of the most common cancers in men is prostate cancer (Jemal et al., 2007). Selenium (Se) is being studied more closely as a potential anticancer drug since it has been hypothesized to have cancer-prevention properties (Kong et al., 2011). Epidemiology, ecology, and medicine have revealed that se reduces the incidence of some malignancies, including breast, colon, lung, and prostate cancer (Helzlsouer et al., 2000; Klein, 2004; El-kassas and El-Sheekh, 2014; El-Sheekh et al., 2021). Ag, Au, TiO_2, $CuCl_2$, CeO_2, and SiO_2 NPs have been evaluated for their antiviral properties against a variety of viruses, including influenza virus H3N2 type-2, hepatitis B virus (HBV), foot-and-mouth disease virus, HIV-1, and H1N1, vesicular stomatitis virus dengue virus and HSV-1 (Rai et al., 2015; Orłowski et al., 2018; El-Sheekh et al., 2022). SeNPs have recently been investigated as antiviral agents for different types of fabrics. To achieve this, the authors of a recent polymer study used a flat screen-printing technique to graft SeNPs onto polyester fabric. They then measured the antimicrobial activity of the resulting material against SARS-CoV-2 *Pseudomonas aeruginosa*, *Bacillus cereus*, *Salmonella typhi*, and *Escherichia coli*. Following an MTT experiment, the researchers discovered that the printed polyester textiles with SeNPs exhibit high antiviral activity and are not harmful to human skin (Abou Elmaaty et al., 2022). It is worth saying that SeNPS were produced by different types of microalgae, like many strains of Cyanobacteria such as *Anabaena variabilis* and *Spirulina platensis* (Afzal et al., 2021; ElSaied et al., 2021), and only from *Ulva lactuca* (Chlorophyta) and *Sargassum latifolium* (Ochrophyta, Phaeophyceae) (El-Khateeb et al., 2019; Vikneshan et al., 2020; Makhlof et al., 2022) and for the first time in this research SeNPS are produced from the brown algae *Polycladia myrica* (formerly *Cystoseira myrica)* (formerly *Polycladia myrica)*. So, this research aims to examine the antiviral and anticancer properties of Se-NPs mediated by *P. myrica* using the PC3 cell line, Herpes simplex II, Hepatitis A, and Adenovirus by MTT test, and the experiment was carried out *in vitro*.

2 Material and methods

2.1 Collection of algal samples

The brown seaweed *Polycladia myrica* was collected from the Gulf of Suez, Egypt coast. Dr. Fekry Ashour Mourad, a researcher at NIOF Egypt, identified the alga. All samples were identified as described previously and according to the methods of Aleem [Aleem, 1978; Aleem, 1993; Lipkin and Silva, 2002) and were confirmed using the Algae Base website (Guiry and Guiry, 2022). Sand and other foreign objects Sand and other foreign objects were removed from the algal samples by washing them under running fresh water. Before being brought to the lab, the seaweed was gathered and put in a polyethylene bag. The seaweed was washed three times with deionized water until the pH of the wash solution was comparable to deionized water. The seaweed was rinsed twice with distilled water to remove any metallic compound. The seaweed was collected, fully dried in the shade at room temperature, powdered in a mechanical grinder, and then put through a 0.2 **mm** screen, according to Soliman (Soliman et al., 2018).

2.2 Preparation and (FTIR) characterization of algal extract

A round flask containing 5 **g** of powdered alga and 50 mL of deionized water was thoroughly agitated on a rotary shaker for an hour before being allowed to boil at 70°C and then cool to room temperature (Hashemi et al., 2015). The extracted solution was filtered using filter paper Whatman No. 1. The filtrate was maintained at 4°C for additional research (Thamer et al., 2018). The spectra between 4000 and 400 nm^{-1} were measured using an FTIR spectrometer (FT/IR-6100 type A). FTIR is used to find the bioactive substances in *Polycladia myrica* extract that cause SeNPs to be bio-reduced and become nanoparticles.

2.3 Preparation of Se nanoparticles

To find the ideal conditions, according to Kashyap (Kashyap et al., 2019), the extract of *Polycladia myrica* was mixed with 1mM Na_2SeO_4 (Sigma Aldrich Company, USA) solution at a mixing ratio (1:9). When the hue of the sodium selenite solution changed to orange-red after being stirred for 72 **h** in the dark at 25 2°C, phycosynthesized PoSeNPs formed (ElSaied et al., 2021). After centrifuging the mixture at 4400 **g** for up to 30 **min**, the NPS was cleaned with double distilled water before being treated with pure ethanol (Murugaboopathy et al., 2021). The finished product was baked at 50°C and kept in a sealed container, to be characterized for research or other purposes (Azizi et al., 2013)..

2.4 PoSeNPs characterization

2.4.1 UV spectroscopy characterization

A spectrophotometer was used to record the CsSeNPs solution's UV-visible spectrum (Thermo Scientific Evolution TM 300) between 200 and 800 nm was used to measure the absorbance.

2.4.2 PoSeNPS' FTIR

FTIR was used to identify the potential active groups of biomolecules that regulate the capping and reduction of nanoparticles. At Al-Azhar University, the Regional Center for

Mycology and Biotechnology in Egypt performed FTIR spectrum analysis using potassium bromide (KBr) as a test substance in the 450–4,000 cm^{-1} wave numbers. The resulting peaks were plotted with wave number (cm^{1}) on the Y-axis and transmittance (percent) on the X-axis.

2.4.3 X-ray diffraction (XRD) spectrum

Utilizing the power of an X-ray diffractometer (XRD-6000, Shimadzu, Japan) with Cu-k radiation (= 1.5412) at 40 KV and 30 mA in the 2 range of 10-80° for purity investigation, the crystallinity and elemental composition of the generated Se-NPs were assessed and characterized.

2.4.4 Transmission electron microscope (TEM)

Using a transmission electron microscope (JEOL, JEM-2100, Japan) running at 200 kV accelerating voltage, the shape, and size of the phycosynthesized SeNPs were studied. Deionized water was used to dilute the reaction solution, and it was then sonicated (Branson-Sonifier 250, USA) for ten min (Tahmasebi et al., 2015). The sonicated sample was dropped onto copper grids coated with carbon before being dried in a vacuum for half an hour; then, we could take electron micrographs (Yue et al., 2004).

2.4.5 SEM scan

SEM stands for the scanning electron microscope. That scans with a high-energy electron beam in a raster scan pattern to bring the picture to the material. The signals produced by the electrons' interactions with the atoms that potentially make up the sample provide information on its surface topography, composition, and other characteristics like electrical conductivity. Laminar airflow and UV light were used to disinfect SeNPs. Using sticky tape, the sterilized nanoparticles were carefully mounted on SEM stubs and evenly covered with gold. The sample was then put into the SEM's sample chamber (JEOL JSM 6490 LV, Japan), and scanning was done at various magnifications between 15,000 and 35,000 and voltages between 20 and 30 kV (Šileikaitė et al., 2009; Razi et al., 2011).

2.4.6 EDX analysis

The biosynthesized selenium nanoparticles were dried and used for XRD analysis to confirm the crystalline nature and phase composition of nanoparticles synthesized using (JSM-IT100, JOEL, Japan) equipped with a LINXEYE detector, operated at 30 kV and 10 mA current with 2.2 KW Cu anode radiation (k = 1.54184 Å). To calculate the average size of the nanoparticles, Scherrer's equation ($D = k\lambda/\beta \cos \theta$) was used, where k is a constant whose value is approximately 0.9, λ is the wavelength of the X-ray (1.54060), β is the width in radians of the peak due to the size effect which is calculated by the following equation: $\beta = \theta_1 - \theta_2 \times \pi/180$ and θ is Bragg's diffraction angle. Specifically, the particle size of the sample was estimated from the line width of the (300) XRD peak.

2.4.7 Zeta potential (ζ)

PoSeNPS surface charges were detected using zeta potential (Zeta plus, Brookhaven, USA). 25 µg of SeNPs samples were diluted in water ten times to prepare the sample, which was then sonicated for 15 min. at 20 Hz. Before measuring the zeta potential, the mixture was passed through a 0.22 m filter. NP aggregation was avoided by diluting SeNPs. Measurements ranged from -200 to +200 mV (ElSaied et al., 2021).

2.5 Antiviral activity test of SeNPs

2.5.1 Mammalian cell line

The American Type Culture Collection provided Vero cells taken from an African green monkey kidney (ATCC, Manassas, VA, USA). DMEM was used to grow Vero cells (Dulbecco's Modified Eagle's Medium), which contained 10% heat-inactivated foetal bovine serum (FBS), 1% L-glutamine, HEPES buffer, and 50 gram per ml gentamycin. All cells are subcultured 2 times weekly and reservation at thirty-seven °C in a moisturizer environment with 5% carbon dioxide (Vijayan et al., 2004).

2.5.2 Virus propagation

In confluent Vero cells, the cytopathogenic HAV HM175 strain of hepatitis A virus, herpes simplex type 2 virus (HSV-2), or adenovirus strain 2 was propagated and tested (Randazzo et al., 2018). The Spearman-Karber method was used to count the number of infectious viruses by calculating the dose of infectious tissue culture (TCID50) by using 8 wells of each dilution and 20 µL of inoculum in each well (Pinto et al., 1994).

2.5.3 Cytotoxicity evaluation

Vero cell lines were planted in 96-well plates for the cytotoxicity experiment at a cell density of 2×10^5 cells in each ml per 100 L medium for growth. Following a day of injection, a new growth medium with different quantities of the tested material was introduced. Monolayers of the confluent cell were distributed into microtiter plates with 96-well and a flat-bottomed using a multichannel pipette (Falcon, Jersey, NJ, USA) in serial duplicated dilutions of the PoSeNPS starting with 3000 g/mL and decreasing down to two g/mL. 48 h were spent incubating the microtiter plates at 37°C in a moisture incubator with 5% carbon dioxide. For each concentration of the tested substance, 3 wells were employed. Cells as control were cultured with or without DMSO and without tested samples. It was discovered that the experiment was unaffected by the minimal aliquot of DMSO (maximum 0.1%) placed in each well. A MTT colorimetric technique was used to determine the

viable cell yield following the conclusion of the incubation time (Mosmann, 1983; Riyadh et al., 2015). In a nutshell, the medium for culturing was withdrawn to be replaced with 100 µ of fresh medium devoid of phenol red. The stock solution with 12 mM MTT was added to each well which was prepared by adding 5 mg of MTT in 1 mL of PBS in the presence of the controls, which was untreated.

For 4 h, the 96-well plates were incubated at 37 °C with 5% carbon dioxide. After 85µl aliquot media were removed from each well, 50 µl DMSO was added and mixed with the pipette carefully then incubation was done at 37 °C for 10 min. The viable cells' number was then determined by measuring the optical density at 590 nm using an ELISA reader (SunRise, TECAN, Inc., USA) to calculate the percentage of viability, where the mean optical density of wells treated with PoSeNPS is ODt, and the mean optical density of untreated cells is ODc. The viability curve of the Vero cell line followed by treatment with the specified drug is obtained by plotting a curve between tested compound concentration and surviving cells. The dose-response curve of each concentration was plotted using the Graphpad Prism software to obtain the 50% cytotoxic concentration (CC50), which is the dosage necessary to produce lethal effects in intact cells (San Diego, CA. USA). For further biological research, each compound's maximum non-toxic concentration (MNT) was also established.

2.5.4 Evaluation of the antiviral activity

At the Regional Center for Mycology and Biotechnology, a cytopathic effect inhibition assay was used for the antiviral screening (RCMB, Al-Azhar University, Cairo, Egypt). The test was chosen to demonstrate the precise suppression of a biological process, specifically the cytopathic effect in sensitive mammalian cells, as evaluated by the MTT technique (Hu and Hsiung, 1989; Al-Salahi et al., 2015). In a nutshell, 96-well microtiter plates containing monolayers of (2×10^5 cells/mL) the adhered Vero cells at the bottom of the wells were incubated for a day at 37°C in a moistened incubator with 5% carbon dioxide.

The SeNPS concentrate simultaneously treated cultures in a fresh maintenance medium after the plates had been rinsed with fresh Dulbecco's Modified Eagle's Medium and challenged with 104 doses of the virus; after this, they were incubated at 37°C for 2 days.

By SeNPS absence, infection controls and an untreated Vero cell control were created. For each concentration of the substance under examination, six wells were employed. The activity of the Antiviral was assessed by comparing the cytopathic inhibition effect to the control, and the level of protection provided to the cells by the test substance was calculated. Four replicates of each treatment were included in each evaluated independent experiment. In this assay technique, the positive controls were amantadine or acyclovir. Following the incubation period, the cells' viability was estimated using the MTT assay, which was previously covered in the cytotoxicity section (Mosmann, 1983).

The rate of viral inhibition could be estimated as follows:

$$\left[\frac{(A-B)}{(C-B)}\right] \times 100\,\%$$

where A, B, and C indicate the absorbance of the SeNPS with virus-infected cells, the virus control absorbance, and the cell control absorbance, respectively.

2.5.5 Data analysis

Using these data and STATA modeling software, the dose that prevented 50% of viral infection (EC50) was calculated concerning virus control from the visual plots. The three tests' median and standard error data show the percentages of viral inhibition concerning each virus under the test. The obtained curve by plotting the inhibition of the viral yield against the concentration of SeNPS was used to calculate EC_{50} values directly. The ratio of CC_{50} to EC_{50} was used to calculate the selectivity index (SI), which was used to examine whether each chemical had enough antiviral activity to outperform its degree of toxicity (Alshalalfeh et al., 2016). This measure, known as a therapeutic index, was also employed to decide if a drug was worthy of further investigation. Active compounds had an SI-value of 2 or higher (Al-Salahi et al., 2015).

2.6 Cytotoxicity of SeNPS against PC-3

2.6.1 Mammalian cell lines

The American Type Culture Collection provided a human prostate cancer cell line (PC-3 cells) (ATCC, Rockville, MD).

2.6.2 Chemicals used

The foetal bovine serum, MTT, trypan blue dye, dimethyl sulfoxide (DMSO), and DMSO were purchased from Sigma (St. Louis, Mo., USA). Lonza was used to purchase RPMI-1640, HEPES buffer solution, L-glutamine, gentamycin, and 0.25% Trypsin-EDTA (Belgium).

2.6.3 Propagation of cell line

Cell culturing was done on growth medium (RPMI-1640) supplemented with ten % inactivated foetal calf serum and 50% gentamycin. The cells were subcultured two to three times every 7 days and kept at 37°C in a moist environment with five % CO_2.

2.6.4 Cytotoxicity evaluation using viability assay

In Corning 96-well tissue culture plates, we suspend tumor cell lines in media with a concentration of 5×10^4 cells per well for antitumor tests and then incubated for 24 h. To produce 10 concentrations of each chemical, the SeNPS were then put into

96-well plates (three duplicates). For every plate with 96 well, six-vehicle controls with media or 0.5% DMSO were run as a control. The MTT test assessed the number of viable cells after 24 h of incubation. In a nutshell, the RPMI 1640 medium without phenol red was replaced with 100 l of fresh culture medium for 96-well plates, and 10 µl of the stock solution of 12 mM MTT (5 mg of MTT in 1 mL of PBS) was set to each well that includes the untreated controls.

The plates with 96-well were then incubated for 4 h at 37°C with five % carbon dioxide. After 85µl aliquot of the media was removed from each well, 50µl of DMSO was added to each well with careful pipette mix, then incubation at 37°C for 10 min was done. The number of viable cells was then determined by measuring the optical density at 590 nm with an ELISA (SunRise, TECAN, Inc., USA). According to the following formula, the viability percentage was calculated [(ODt/ODc)] x100%, where ODt is the mean optical density of wells treated with SeNPS and ODc is the mean optical density of control untreated cells. After adding the given substance, the curve between viable cells and the concentration drug is displayed to determine the viability curve of each cancer cell line. Utilizing Graphpad Prism software (San Diego, CA, USA), from graphic plots of the dose-response curve for each conc, we could calculate the concentration of fifty % inhibition (IC_{50}), or the needed concentration to have harmful effects in fifty % of intact cells (Mosmann, 1983).

2.6.5 Microscopic observation of the prostate carcinoma (PC3) cell line treated with the PoSeNPS

The protocol for cytotoxic activity was followed during the conduct of this experiment. After the treatment at the tested concentration was complete, after removing the medium from the plates, the wells were washed three times with 300µL of phosphate-buffered saline (pH 7.2). We can fix the cells to the plate for fifteen min with 10% formalin at room temperature. After that, 100 µl of crystal violet with a concentration of 0.25% was used to make staining for the fixed cells for 20 min. After the stain was eliminated, we should rinse the plates with dH_2O to remove any remaining color, and then they were left to dry. Images showing morphological alterations compared to control cells were taken by using an inverted microscope (CKX41; Olympus, Japan), which was supplied with a digital camera for microscopy. At a magnification of 200x, the cytopathic effects (morphological changes) were visible.

3 Result and discussion

3.1 FTIR characterization of algal extract

According to the FTIR analysis of *P. myrica* extract (Figure 1), the presence of phenol or alcohol molecules is indicated by an absorption band at 3405 cm^{-1} of strong stretching –OH (Silva et al., 2014; Hu et al., 2016; Mohamed et al., 2021). The peak at 2926 cm-1 represents the N=C=S stretching bond (isothiocyanate); also, the CH2 anti-symmetric stretch of methyl groups in lipids caused the absorption bands at 2977–2852 cm^{-1} (Lu and Rasco, 2012). Due to the N-H bending vibration of secondary amines and the carbonyl unsaturated ketone amide (lipid, protein), the absorption bands at 1628 cm^{-1} indicate the stretching vibration of -C=O- of Amide I. This agrees with Demir (Demir et al., 2015), who discovered that bands at 1739-1638 cm^{1} of the spectra show the stretching of C=C of phenyl compounds and the stretching of C=O of aromatic.

The lignin or asymmetric stretching vibration of nitro compounds (N-O) is indicated by the absorbance band at 1509 cm^{1}, representing the stretching vibration of C = C. Kubi and Kadla (Kubo and Kadla, 2005). Lopez (López et al., 2014) notice a

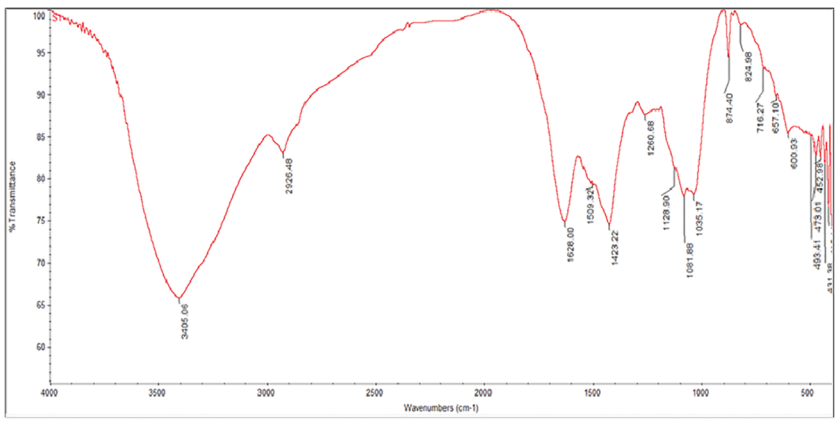

FIGURE 1
FTIR spectra of *Polycladia myrica* aqueous extract.

small amount of lignin in seaweed cell walls. Furthermore, lignin's cytotoxic properties against colon cancer were demonstrated by Lue (Lu et al., 1998). The absorption band indicated the existence of carboxylic acid (O-H bending) at 1423 cm^{-1}. Younger (Younger, 2014) It was well known that seaweed had many carboxylic acids, especially fatty acids. Deyab (Deyab et al., 2012). described the anticancer effects (*in vitro*) of several fatty acids, such as (oleic and palmitic acids) from seaweed. The primary and secondary amines' N-H stretching is indicated by the 1260 absorbance band (ElSaied et al., 2021). According to Singh and ElSaied (Singh et al., 2016; ElSaied et al., 2021), the absorbance band at 1081 cm ^{1} demonstrate the stretching of carbohydrates' C-O, like pectin and starch, and the stretching vibration of C-N of aliphatic amines. 1128 cm^{1} band is attributable to ACH_2OH groups of carbohydrates (Mordechai et al., 2001). Chowdhury discovered Fenugreek seed was high in the polysaccharide galactomannan in 1987 (Chowdhury et al., 1987). Plant extracts, including phenol and flavonol derivatives, function as reducing agents and nanoparticle stabilizers and have been implicated in the reduction of selenious acids to SeNPs (Huang et al., 2004).

The absorption bands at 600-716 cm^{-1} (Phaeophyceae and Chlorophyta) show the stretching of C = S, which suggests sulfides in the tested algae. C-Br stretching peaks at 600 cm343 at 3405 cm^{-1} belonging to the aqueous extract of *C. myrica* was shifted to the phycosynthesized represented alkyl halides compound (lipids) (Younger, 2014). Based on these findings, we discovered that *P. myrica* included a variety of phytochemicals, including phenol, alcohol, lipid, proteins, fatty acids, and other substances with anticancer and antiviral properties. Additionally, these phytochemicals might have helped sodium selenite convert to SeNAPS (Huang et al., 2007; Vikneshan et al., 2020).

3.2 Nanoparticles characterization

The results of SeNPS have been validated using seven characterization techniques: UV-Vis spectra, FTIR, XRD, TEM scanning, SEM scanning, EDX, and zeta potential.

3.2.1 SPR characteristic

Studies using UV-Vis spectra confirmed that sodium selenite's color changed from colorless to ruby red (SeNPs), and that this color change was caused by the biosynthesis of SeNPs (Figure 2). As PoSeNPS decreased, the absorbance steadily climbed from 1.9 to 3. The largest beak, though, was discovered to be 350 nm.

3.2.2 PoSeNPS' FTIR analysis

To look into the functional groups responsible for the synthesis and stability of nanoparticles, the biosynthesized PoSeNPS were examined by FTIR analysis (Figure 3). Due to the aromatic rings' -OH stretching and the presence of alcohol and phenol groups, the marker bands of SeNPs (powder) exhibit an absorption peak at 3300 cm^{-1} and a peak at 2927 cm^{-1} because of the stretching vibration of C-H of alkenes. These peaks demonstrate the presence of a biopolymer that is likely derived from the algal cell walls and is connected with the SeNPs (Fritea et al., 2017). Additionally, the amide I and II bands may be seen at 1652 cm^{-1} for the C=O stretch of the ester group and 1543 cm^{-1} for the N-H bending of the amines primary and secondary, respectively. Bands of 1321 cm^{-1} and CH2 and CH3 groups exhibit asymmetric C-H bending (Fritea et al., 2017; ElSaied et al., 2021). According to the literature, another absorption band at 1036 cm^{-1} shows the superposition of in-plane C-H bending and C-N stretching vibration of aliphatic amines and the distinctive Se-O stretching vibration (Kannan et al., 2014). At 698 and 468 cm^{-1}, further bending vibrations of the Se-O bond are highlighted. The peak at 3405 cm^{-1} belonging to the aqueous extract of *P. myrica* was shifted to the phycosynthesized PoSeNPS peak at 3300 cm^{-1}, as shown in Figure 3 (Gunti et al., 2019). This indicated the interaction between Se and hydroxyl group from the *P. myrica* aqueous extract through hydrogen bonding which facilitated phycosynthesized CsSeNPs. Similar to this, the sharp peaks at 1628 and 1509 cm^{-1}, that responsible for the stretching of C=O and nitro asymmetric stretching vibration (N-O) compounds in the *C. myrica* extract, were both shifted to higher frequencies at 1652 and 1543 cm^{-1}, respectively, in phycosynthesized PoSeNPS, showing the interaction between carbonyl C=O stretch and N-O

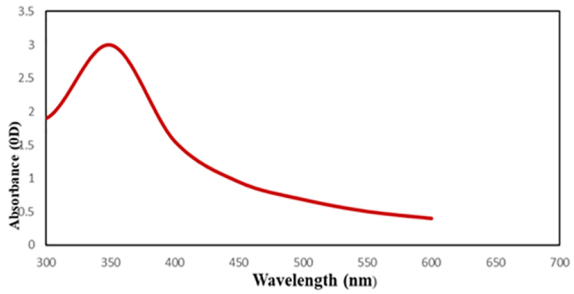

FIGURE 2
UV-Visible spectrum of PoSeNPs.

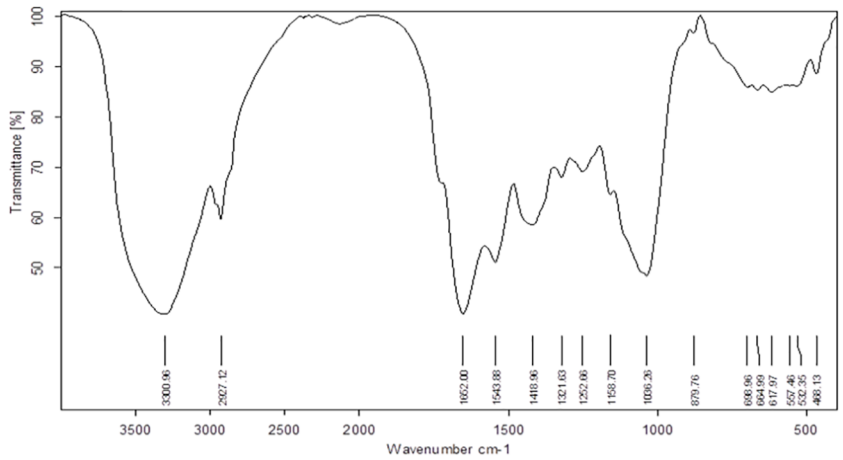

FIGURE 3
FTIR spectra of PoSeNPs.

compounds of *P. myrica* aqueous extract with Se. The protein character of phycosynthesized PoSeNPS, which may be in charge of reduction and stabilization, is indicated by 2 absorption peaks of C-N stretching vibration of aliphatic amines and the N-H stretching of the primary and secondary amines at 1081 and 1260 cm^{-1}, respectively (Kokila et al., 2017). From the FTIR, it can be deduced that the bio-organic components of *P. myrica* extract, such as carbonyl-unsaturated ketone amides, amino acids, esters, and proteins, acted as potent capping and reducing agents on PoSeNPs (Liu et al., 2013). Similar findings have previously been published concerning these functional biochemical bonds (Suganya et al., 2015).

3.2.3 XRD analysis

Utilizing the XRD techniques depicted in Figure 4, it was possible to identify SeNPS's crystal structure and phase composition. The sample's XRD pattern implies that it is nanocrystalline and closely resembles the typical selenium powder, indicating that selenium particles were formed. There is a specific diffraction peak in the range of 14–52.4° at the angle of 2θ, which is consistent with the diffraction peak of (JCPDS card number 65-1290). It can be inferred that the obtained particles are selenium. The diffraction peak in the pattern is very narrow, indicating that the synthesized nano-

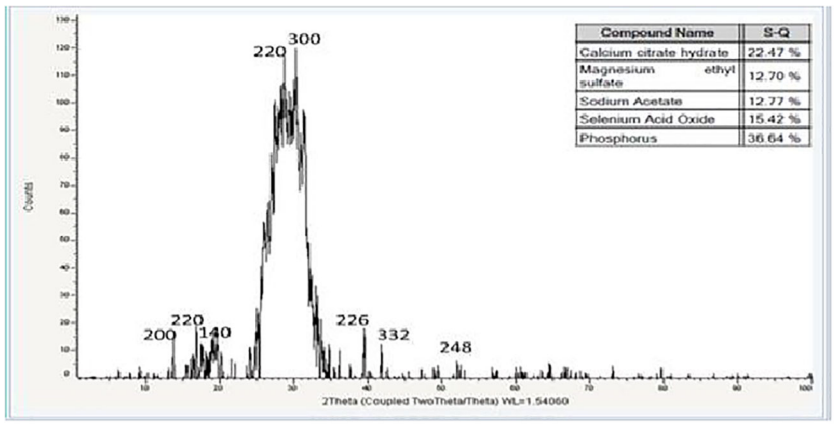

FIGURE 4
XRD spectrum of PoSeNPs.

selenium particles are very small in size, crystalline, and with poor amorphous character. The XRD patterns obtained show the main peaks characteristic of crystalline SeNPS at 2θ values of 14°, 17.4°, 20.14°, 28.5°, 30°, 39.42°, 42.4°, and 52.4° (Figure 4) corresponding to the crystal planes (200), (220), (140), (220), (300), (226), (332) and (248), respectively. The average crystalline size of biogenic Se nanostructures measured by Scherrer's equation was about 15.9 nm. The biological approach of SeNPs produced some background noise, which may have been caused by the presence of additional bioactive compounds in the *P. myrica* extract (Figure 4). The powder's XRD pattern demonstrates that post-annealing is unnecessary to achieve the desired crystalline phase (ElSaied et al., 2021).

3.2.4 Transmission Electron Microscopy (TEM) imaging

It has been established that the physical and chemical properties of the synthesized SeNPS, such as crystalline structure, shape, size dispersion, and surface condition, determine their applicability (Salih et al., 2016). SeNAPS were measured using TEM to establish their size and form, and the results showed that they ranged in size from 9.31 to 68.65 nm and had smooth spherical and semispherical shapes (Figure 5). These findings concur with those of (Vikneshan et al., 2020) and (ElSaied et al., 2021), who synthesized SeNPS using *Ulva lactuca* and *Arthrospira platensis* extracts. They discovered that the morphology of SeNPS using TEM was smooth, spherical/ball-shaped, and distributed uniformly.

3.2.5 SEM imaging

Figure 6 depicts the size of the SeNPS that *P. myrica* produced. The SeNPS's SEM pictures revealed that it had a smooth surface and an oval-to-spherical form. 18.7 to 22.79 nm were found to be

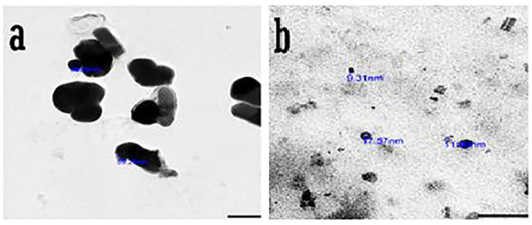

FIGURE 5
Transmission Electron Microscope (TEM) photographs of PoSeNPs **(A, B)** with magnifying field 100nm and diameter.

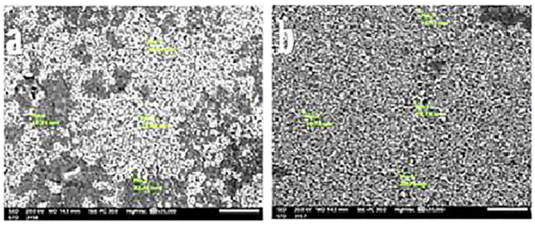

FIGURE 6
Scanning Electron Microscope (SEM) photographs **(A, B)** of PoSeNPs with measuring the diameter of PoSeNPs.

the particle size. The dynamic light scattering approach correlates with SEM analysis and is used for the size-distribution analysis.

3.2.6 EDX analysis

Se atoms were detected in the elemental composition analysis using EDX (atom % 0.11 ± 0.02; mass % 0.56 ± 0.10). (Figure 7). This study revealed the presence of selenium-containing nanostructures together with other EDX peaks like Si, Mg, Na, Ca, and O peaks, indicating that they were mixed

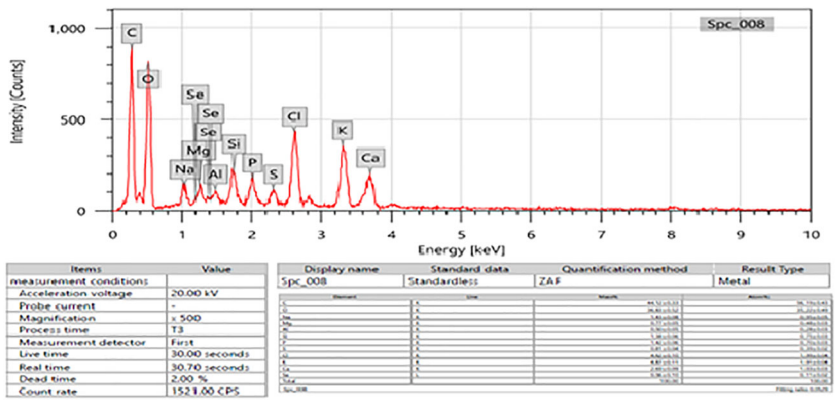

Items	Value
measurement conditions	
Acceleration voltage	20.00 kV
Probe current	-
Magnification	x 500
Process time	T3
Measurement detector	First
Live time	30.00 seconds
Real time	30.70 seconds
Dead time	2.00 %
Count rate	1521.00 CPS

Display name	Standard data	Quantification method	Result Type
Spc_008	Standardless	ZAF	Metal

FIGURE 7
EDX analysis of PoSeNPs3.3.

precipitates of the selenium salt. XRD provided additional evidence that SeNPS were produced.

3.2.7 Zeta potential (ζ)

ζ indicates an estimation of the created electric double layer in the solution by the surrounding ions, not the actual charge on each molecule. Because of the inter-particle electrostatic repulsion, NPs with ζ values between +30 mV to -30 mV typically display stability with high degrees (Jummes et al., 2020). The negative charge of the produced PoSeNPs was validated, indicating better stability of the NPs without aggregation. Zeta potential (Figure 8) was used in the current study to find the potential of the nanoparticles. A change of - 24.0 ± 5.62 mV was made to the zeta potential. With a particle size of 11.17–12.74 nm, SeNPs recorded a λ maximum at 545 nm. Further tests were conducted on the best nanocomposite (PoSeNPs), made from Na_2SeO_3 with extremely small particle sizes.

3.3 Antiviral activity of the SeNPs

To detect the antiviral activity of PoSeNPs against HAV-10, HSV-2, and Adenovirus, MTT assay was used (Table 1) and VERO cell line (Table 2). Table 1 shows the Cytotoxic activity of PoSeNPs with Mammalian cells from African Green Monkey Kidney (Vero) cells detected under these experimental conditions with fifty % cell cytotoxic concentration (CC_{50}) = 220.53 ± 6.89 μg/mL. Table 1 shows that PoSeNPs have antiviral activity with MNCC (50 μg/mL) for all tested viruses. This cytotoxic activity was moderate (++) against the HAV-10 virus with (40.25 ± 2.61%) inhibition and weak (+) against HSV-2 and Adeno virus with (17.39 ± 1.45% and 8.64 ± 0.82%) inhibition, respectively. The best antiviral activity of PoSeNPs was against (HAV-10) with EC_{50} and SI (63.81 ± 2.93 and 3.5), respectively. PoSeNPs show weak EC_{50} in Inactive SI against both HSV-2 and Adenovirus. Xia (Xia et al., 2022) found that Se nanoparticles inhibit infection of Madin–Darby canine kidney (MDCK) cells with H1N1 by preventing chromatin condensation and DNA fragmentation. The antiviral activity of Se NPs against various other types of viruses is probably owing to the Se NPs' direct binding to viral envelope glycoproteins, which prevents viral entry into the host cell, even though the mechanism of action has not been well studied (Lu et al., 2008; Fayaz et al., 2012).

3.4 PoSeNPs cytotoxic activity

Using vero cell lines, PC-3 cell lines were treated with varying doses of CsSeNPs (3.9–50 0 g/mL), and the

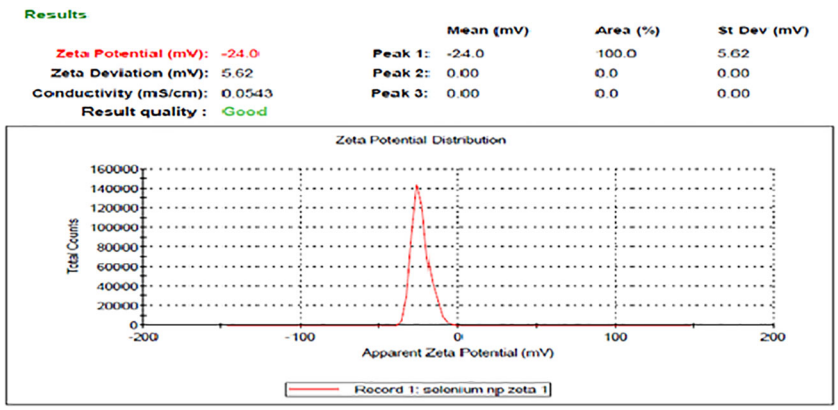

FIGURE 8
Zeta potential of the PoSeNPs.

TABLE 1 The antiviral effects of PoSeNPS when tested at (MNCC).

virus name	MNCC (μg/mL)	Antiviraleffect on HAV-10(%)	Antiviraleffect on HAV-10 (Qualitative)*	Antiviral Efficiency	
				EC_{50}	SI
HAV-10	50	40.25 ± 2.61	++	63.81 ± 2.93	3.5
Adeno virus	50	8.64 ± 0.82	+	Weak activity	Inactive
HSV-2	50	17.39 ± 1.45	+	Weak activity	Inactive

Where (-): No antiviral activity (+): Weak antiviral activity (1-<25%). (++): Moderate antiviral activity (25≤50%).

TABLE 2 The Cytotoxic activity against Mammalian cells from African Green Monkey Kidney (Vero) with 50% cell cytotoxic concentration (CC_{50}) = 220.53 ± 6.89 µg/ml.

Sample conc. (µg/mL)	Viability %	Inhibitory %
0	100	0
3.9	100	0
7.8	100	0
15.6	100	0
31.25	99.76	0.24 ± 0.22
62.5	94.20	5.8 ± 1.34
125	78.39	21.61 ± 2.97
250	41.26	58.74 ± 2.82
500	19.47	80.53 ± 1.65

The data are expressed in the form of mean ±.

cytotoxicity (Table 3 and Figures 9A, B) occurred in a concentration-dependent manner. Clinical trial preliminary findings indicate that dose and Se forms are essential for its anticancer effectiveness (Kong et al., 2011). All concentrations examined exhibit cytotoxic activity, except for 93.9-7.8-15.6 g/mL, which exhibits 100% cell viability and 0% inhibition.

TABLE 3 Inhibitory activity of PoSeNPS against prostate carcinoma cells (PC-3) with IC_{50} = 123.51 ± 4.07 µg/mL.

Sample conc. (µg/ml)	Viability %	Inhibitory %
0	100	0
3.9	100	0
7.8	100	0
15.6	100	0
31.25	98.15	1.85 ± 0.79
62.5	81.72	18.28 ± 2.06
125	49.23	50.77 ± 3.15
250	30.67	69.33 ± 2.49
500	13.85	86.15 ± 2.31

The data are expressed in the form of mean ±.

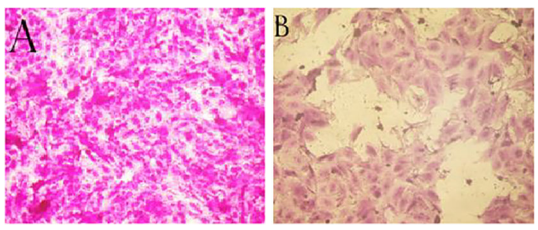

FIGURE 9
(A) PC-3 cells non-treated (control) **(B)** PC-3 cells treated with PoSeNPS at 500 µg/mL concentration.

Kong (Kong et al., 2011) discovered that SeNPS inhibit prostate cancer cells' growth partially *via* caspases-mediated apoptosis. For suppressing cancer growth apoptosis is an important mechanism, and caspases, in turn, induced apoptosis, as shown by the difference between the (9A) image (control cells without treatment and with 100% cell viability) and (9B) image (the cells with the highest PoSeNPS concentration500 µg/mL and 13.85% cell viability) and suppress androgen receptor transcriptional activity by its mRNA down-regulating and protein expression. Furthermore, selenium nanoparticles increase Akt kinase phosphorylation to be activated; therefore, phosphorylation promotes Akt-dependent androgen receptor, and regulation of Mdm2 degradation *via* the proteasome and prostate cancer pathway cell growth suppression by the disruption of androgen receptor, acting as a promising application in cancer therapy.

4 Conclusion

This study concluded that selenium nanoparticles synthesized by the brown alga *Polycladia myrica* have good antiviral activity against HAV-10 virus with an antiviral percent of 40.25%, despite weak antiviral activity against Adenovirus and HSV-2 with antiviral percent (8.64% and 17.39%), respectively. The cytotoxicity effect of these nanoparticles was determined against PC-3 with a maximum inhibitory percent of 80.53%. These nanoparticles have no hazardous effect against normal Vero cells as the viability percent was (78.39% and 49.23%) for Vero cells and PC-3 cells, respectively, at 125 µg/mL. As a suggestion, because each tool used for synthesizing green nanoparticles has its own characteristics, optimizing many factors like pH, materials concentration, and incubation time could increase obtaining more small-sized NPs.

Data availability statement

The original contributions presented in the study are included in the article/supplementary material. Further inquiries can be directed to the corresponding author.

Author contributions

MM carried out the experiments, constructed the Figurers and tables, and wrote the first draft of the manuscript. ME-S and HT shared the research idea, wrote, edited the manuscript, and revised the data and the whole work. All authors have read and agreed to the published version of the manuscript.

Funding

Under grant No IFPIP: 178-662-1443, this project was funded by Institutional Fund Projects, Deanship of Scientific Research (DSR) at King Abdulaziz University, Jeddah.

Acknowledgments

This research work was funded by Institutional Fund Projects under grant no: (IFPIP: 178-662-1443). The authors gratefully acknowledge technical and financial support provided by the Ministry of Education and King Abdulaziz University, DSR, Jeddah, Saudi Arabia.

Conflict of interest

The authors declare that the research was conducted in the absence of any commercial or financial relationships that could be construed as a potential conflict of interest.

Publisher's note

All claims expressed in this article are solely those of the authors and do not necessarily represent those of their affiliated organizations, or those of the publisher, the editors and the reviewers. Any product that may be evaluated in this article, or claim that may be made by its manufacturer, is not guaranteed or endorsed by the publisher.

References

Abou Elmaaty, T., Sayed-Ahmed, K., Elsisi, H., Ramadan, S. M., Sorour, H., Magdi, M., et al. (2022). Novel antiviral and antibacterial durable polyester fabrics printed with selenium nanoparticles (SeNPs). *Polymers.* 14 (5), 1–14. doi: 10.3390/polym14050955

Afzal, B., Yasin, D., Naaz, H., Sami, N., Zaki, A., Rizvi, M. A., et al. (2021). Biomedical potential of anabaena variabilis NCCU-441 based selenium nanoparticles and their comparison with commercial nanoparticles. *Sci. Rep.* 11 (1), 13507. doi: 10.1038/s41598-021-91738-7

Alaqad, K., and Saleh, T. A. (2016). Gold and silver nanoparticles: Synthesis methods, characterization routes and applications towards drugs. *J. Environ. Anal. Toxicol.* 6 (4), 1–10. doi: 10.4172/2161-0525.1000384

Aleem, A. A. (1978). Contribution to the study of the marine algae of the red sea. I–The algae in the neighborhood of al–Ghardaqa, Egypt (Cyanophyceae, chlorophyceae and phaeophyceae). *Bull. Faculty. Sci. King. Abdulaziz. Univ. Jeddah.* 2, 73–88.

Aleem, A. A. (1993). *Marine algae in Alexandria, Egypt* (Alexandria, VA, USA: Alexandria Privately Published), 1–135.

Al-Salahi, R., Alswaidan, I., Ghabbour, H. A., Ezzeldin, E., Elaasser, M., and Marzouk, M. (2015). Docking and antiherpetic activity of 2-aminobenzo[de]-isoquinoline-1,3-diones. *Molecules* 20 (3), 5099–5111. doi: 10.3390/molecules20035099

Alshalalfeh, M. M., Sohail, M., Saleh, T., and Aziz, M. (2016). Electrochemical investigation of gold nanoparticle-modified glassy carbon electrode and its application in ketoconazole determination. *Aust. J. Chem.* 69 (11), 1314–1320. doi: 10.1071/CH16072

Anwar, N., Khan, A., Shah, M., Azam, A., Zaman, K., and Parven, Z. (2016). The green synthesis of fine particles of gold using an aqueous extract of monotheca buxifolia (Flac.). *Russian J. Phys. Chem. A.* 90 (13), 2625–2632. doi: 10.1134/s003602441613015x

Anwar, N., Wahid, J., Uddin, J., Khan, A., Shah, M., Shah, S. A., et al. (2021). Phytosynthesis of poly (ethylene glycol) methacrylate-hybridized gold nanoparticles from c. tuberculata: their structural characterization and potential for *in vitro* growth in banana. *In. Vitro Cell. Dev. Biol. - Plant* 57 (2), 248–260. doi: 10.1007/s11627-020-10150-4

Arshad, M., Khan, A., Farooqi, Z. H., Usman, M., Waseem, M. A., Shah, S. A., et al. (2017). Green synthesis, characterization and biological activities of silver nanoparticles using the bark extract of *Ailanthus altissima*. *Mater. Science-Poland.* 36 (1), 21–26. doi: 10.1515/msp-2017-0100

Arya, A., Gupta, K., Chundawat, T. S., and Vaya, D. (2018). Biogenic synthesis of copper and silver nanoparticles using green alga botryococcus braunii and its antimicrobial activity. *Bioinorg. Chem. Appl.* 2018, 7879403. doi: 10.1155/2018/7879403

Azizi, S., Namvar, F., Mahdavi, M., Ahmad, M. B., and Mohamad, R. (2013). Biosynthesis of silver nanoparticles using brown marine macroalga, sargassum muticum aqueous extract. *Mater. (Basel).* 6 (12), 5942–5950. doi: 10.3390/ma6125942

Bhuyar, P., Rahim, M. H. A., Sundararaju, S., Ramaraj, R., Maniam, G. P., and Govindan, N. (2020). Synthesis of silver nanoparticles using marine macroalgae *Padina* sp. and its antibacterial activity towards pathogenic bacteria. *Beni-Suef. Univ. J. Basic. Appl. Sci.* 9 (1), 3. doi: 10.1186/s43088-019-0031-y

Bisht, N., Phalswal, P., and Khanna, P. K. (2022). Selenium nanoparticles: a review on synthesis and biomedical applications. *Mater. Adv.* 3 (3), 1415–1431. doi: 10.1039/d1ma00639h

Chowdhury, S., Ahmed, H., and Chatierjee, B. P. (1987). Purification and characterization of an a-d-galactosyl-binding lectin from *Artocarpus lakoocha* seeds. *Carbohydr. Res.* 159, 137–148. doi: 10.1016/S0008-6215(00)90011-9

Demir, P., Onde, S., and Severcan, F. (2015). Phylogeny of cultivated and wild wheat species using ATR-FTIR spectroscopy. *Spectrochim. Acta A. Mol. Biomol. Spectrosc.* 135, 757–763. doi: 10.1016/j.saa.2014.07.025

Deyab, M. A., Habbak, L. Z., and Ward, F. M. (2012). Antitumor activity of water extract and some fatty acids of turbinaria ornata (Turner) j. agardh. *Egypt. J. Exp. Biol. (Bot.)* 8 (2), 199–204.

El-kassas, H. Y., and El-Sheekh, M. M. (2014). Cytotoxic activity of biosynthesized gold nanoparticles with an extract of the red seaweed *Corralina officinalis* on human breast cancer (MCF-7) cell line. *Asian Paci. J. Cancer Prev.* 9), 4311–4317. doi: 10.7314/APJCP.2014.15.10.4311

El-Khateeb, A., Hamed, E., Ibrahim, F., and Hamed, S. (2019). Eco-friendly synthesis of selenium and zinc nanoparticles with biocompatible sargassum latifolium algae extract in preservation of edible oils. *J. Food Dairy. Sci.* 10 (5), 141–146. doi: 10.21608/jfds.2019.43131

ElSaied, B. E. F., Diab, A. M., Tayel, A. A., Alghuthaymi, M. A., and Moussa, S. H. (2021). Potent antibacterial action of phycosynthesized selenium nanoparticles using spirulina platensis extract. *Green Process. Synthesis.* 10 (1), 49–60. doi: 10.1515/gps-2021-0005

El-Shanshoury, A. R., Darwesh, O. M., Sabae, S. Z., Awadallah, M. A., and Hassan, S. H. (2020). Bio-manufacturing of selenium nanoparticles by *Bacillus subtilis* isolated from qarun lake and evaluation their activity for water remediation. *Biointerface. Res. Appl. Chem.* 10, 5834–5842. doi: 10.33263/BRIAC104.834842

El-Sheekh, M. M., and El-Kassas, H. Y. (2016). Algal production of nano-silver and gold: Their antimicrobial and cytotoxic activities: A review. *J. Genet. Eng. Biotechnol.* 14 (2), 299–310. doi: 10.1016/j.jgeb.2016.09.008

El-Sheekh, M., Hassan, L. H., and Morsi, H. H. (2021). Assessment of the *in vitro* anticancer activities of cyanobacteria mediated silver oxide and gold nanoparticles in human colon CaCo-2 and cervical HeLa cells. *Environ. Nanotechnol. Monit. Manage.* 16, 100556. doi: 10.1016/j.enmm.2021.100556

El-Sheekh, M. M., Shabaan, M. T., Hassan, L., and Morsi, H. H. (2022). Antiviral activity of algae biosynthesized silver and gold nanoparticles against Herps simplex (HSV-1) virus in vitro using cell-line culture technique. *Int. J. Environ. Health Res.* 32 (3), 616–627. doi: 10.1080/09603123.2020.1789946

Fayaz, A. M., Ao, Z., Girilal, M., Chen, L., Xiao, X., Kalaichelvan, P., et al. (2012). Inactivation of microbial infectiousness by silver nanoparticles-coated condom: a

new approach to inhibit HIV- and HSV-transmitted infection. *Int. J. Nanomed.* 7, 5007–5018. doi: 10.2147/IJN.S34973

Fritea, L., Laslo, V., Simona, C., Traian, C., and Simona, V. (2017). Green biosynthesis of selenium nanoparticles using parsley (*Petroselinum crispum*) leaves extract. *Studia. Univ. Vasile. Goldis. Arad. Seria. Stiintele. Vietii.* 27, 203–208.

Guiry, M. D., and Guiry, G. M. (2022). *AlgaeBase* (WorldWide Electronic Publication. National University of Ireland). Available at: https://www.algaebase.org.

Gunalan, S., Sivaraj, R., and Rajendran, V. (2012). Green synthesized ZnO nanoparticles against bacterial and fungal pathogens. *Prog. Natural Sci.: Mater. Int.* 22 (6), 693–700. doi: 10.1016/j.pnsc.2012.11.015

Gunti, L., Dass, R. S., and Kalagatur, N. K. (2019). Phytofabrication of selenium nanoparticles from emblica officinalis fruit extract and exploring its biopotential applications: Antioxidant, antimicrobial, and biocompatibility. *Front. Microbiol.* 10. doi: 10.3389/fmicb.2019.00931

Hashemi, S. A., Madani, S. A., and Abediankenari, S. (2015). The review on properties of aloe Vera in healing of cutaneous wounds. *BioMed. Res. Int.* 2015, 714216. doi: 10.1155/2015/714216

Hatfield, D. L., Tsuji, P. A., Carlson, B. A., and Gladyshev, V. N. (2014). Selenium and selenocysteine: roles in cancer, health, and development. *Trends Biochem. Sci.* 39 (3), 112–120. doi: 10.1016/j.tibs.2013.12.007

Helzlsouer, K. J., Han-Yao, H., Alberg, A. J., Sandra Hoffman, A. B., Edward, P., Norkus, J. S. M., et al. (2000). Association between alpha-tocopherol, gamma-tocopherol, selenium, and subsequent prostate cancer. *J. Natl. Cancer Inst.* 92 (24), 2018–2023. doi: 10.1093/jnci/92.24.2018

Huang, J., Li, Q., Sun, D., Lu, Y., Su, Y., Yang, X., et al. (2007). Biosynthesis of silver and gold nanoparticles by novel sundriedCinnamomum camphoraleaf. *Nanotechnology* 18 (10), 285–290. doi: 10.1088/0957-4484/18/10/105104

Huang, H., Yuan, Q., and Yang, X. (2004). Preparation and characterization of metal-chitosan nanocomposites. *Colloids. Surf. B. Biointerfaces.* 39 (1-2), 31–37. doi: 10.1016/j.colsurfb.2004.08.014

Hu, J. M., and Hsiung, G. D. (1989). Evaluation of new antiviral agents: I. *In vitro* perspectives. *Antiviral Res.* 11, 217–232. doi: 10.1016/0166-3542(89)90032-6

Hu, Y., Pan, Z. J., Liao, W., Li, J., Gruget, P., Kitts, D. D., et al. (2016). Determination of antioxidant capacity and phenolic content of chocolate by attenuated total reflectance-Fourier transformed-infrared spectroscopy. *Food Chem.* 202, 254–261. doi: 10.1016/j.foodchem.2016.01.130

Jemal, A., Siegel, R., Ward, E., Murray, T., Xu, J., and Thun, M. J. (2007). Cancer statistics 2007. *CA Cancer J. Clin.* 57, 43–66. doi: 10.3322/canjclin.57.1.43

Jummes, B., Sganzerla, W. G., da Rosa, C. G., Noronha, C. M., Nunes, M. R., Bertoldi, F. C., et al. (2020). Antioxidant and antimicrobial poly-ϵ-caprolactone nanoparticles loaded with cymbopogon martinii essential oil. *Biocatalysis. Agric. Biotechnol.* 23, 101499. doi: 10.1016/j.bcab.2020.101499

Kannan, S., Mohanraj, K., Prabhu, K., Barathan, S., and Sivakumar, G. (2014). Synthesis of selenium nanorods with assistance of biomolecule. *Bull. Mater. Sci.* 37, 1631–1635. doi: 10.1007/s12034-014-0712-z

Kashyap, M., Samadhiya, K., Ghosh, A., Anand, V., Shirage, P. M., and Bala, K. (2019). Screening of microalgae for biosynthesis and optimization of Ag/AgCl nano hybrids having antibacterial effect. *RSC. Adv.* 9 (44), 25583–25591. doi: 10.1039/c9ra04451e

Khalifa, S. A. M., Elias, N., Farag, M. A., Chen, L., Saeed, A., Hegazy, M. F., et al. (2019). Marine natural products: A source of novel anticancer drugs. *Mar. Drugs* 17 (9), 2–31. doi: 10.3390/md17090491

Klein, E. A. (2004). Selenium: epidemiology and basic science. *J. Urol.* 171 (2 Pt 2), S50–S53. doi: 10.1097/01.ju.0000107837.66277.e9

Kokila, K., Elavarasan, N., and Sujatha, V. (2017). Diospyros montana leaf extract-mediated synthesis of selenium nanoparticles and their biological applications. *New J. Chem.* 41 (15), 7481–7490. doi: 10.1039/c7nj01124e

Kong, L., Yuan, Q., Zhu, H., Li, Y., Guo, Q., Wang, Q., et al. (2011). The suppression of prostate LNCaP cancer cells growth by selenium nanoparticles through Akt/Mdm2/AR controlled apoptosis. *Biomaterials* 32 (27), 6515–6522. doi: 10.1016/j.biomaterials.2011.05.032

Kubo, S., and Kadla, J. (2005). Hydrogen bonding in lignin: A Fourier transform infrared model compound study. *Biomacromolecules* 6, 2815–2821. doi: 10.1021/bm050288q

Kulkarni, N., and Muddapur, U. (2014). Biosynthesis of metal nanoparticles: A review. *J. Nanotechnol.* 2014, 1–8. doi: 10.1155/2014/510246

Labunskyy, V. M., Hatfield, D. L., and Gladyshev, V. N. (2014). Selenoproteins: molecular pathways and physiological roles. *Physiol. Rev.* 94 (3), 739–777. doi: 10.1152/physrev.00039.2013

Lipkin, Y., and Silva, P. C. (2002). Marine algae and seagrasses of the dahlak archipelago, southern red Sea. *Nova. Hedwigia.* 75 (1-2), 1–90. doi: 10.1127/0029-5035/2002/0075-0001

Liu, H., Xu, H., and Huang, K. (2017). Selenium in the prevention of atherosclerosis and its underlying mechanisms. *Metallomics* 9 (1), 21–37. doi: 10.1039/c6mt00195e

Liu, H. J., Xu, C. H., Li, W. M., Wang, F., Zhou, Q., Li, A., et al. (2013). Analysis of spirulina powder by Fourier transform infrared spectroscopy and calculation of protein content. *Guang. Pu. Xue. Yu. Guang. Pu. Fen. Xi.* 33 (4), 977–981. doi: 10.3964/j.issn.1000-0593(2013)04-0977-05

López, M., Moral, A., Aguado, R., Campaña, L., and Tijero, A. (2014). Evaluation of bloom algae as raw material for papermaking. *13th European Workshop on Lignocellulosics and Pulp.* (Seville, Spain) 1.

Lu, F. J., Chu, L. H., and Gau, R. J. (1998). Free radical-scavenging properties of lignin. *Nutr. Cancer* 30 (1), 31–38. doi: 10.1080/01635589809514637

Lu, X., and Rasco, B. A. (2012). Determination of antioxidant content and antioxidant activity in foods using infrared spectroscopy and chemometrics: a review. *Crit. Rev. Food Sci. Nutr.* 52 (10), 853–875. doi: 10.1080/10408398.2010.511322

Lu, L., Sun, R. W.-Y., Chen, R., Hui, C.-K., Ho, C.-M., Luk, J. M., et al. (2008). Silver nanoparticles inhibit hepatitis b virus replication. *Antiviral Ther.* 13 (2), 253–262. doi: 10.1177/135965350801300210

Makhlof, M. E. M., Albalwe, F. M., Al-Shaikh, T. M., and El-Sheekh, M. M. (2022). Suppression effect of ulva lactuca selenium nanoparticles (USeNPs) on HepG2 carcinoma cells resulting from degradation of epidermal growth factor receptor (EGFR) with an evaluation of its antiviral and antioxidant activities. *Appl. Sci.* 12 (22), 11546. doi: 10.3390/app122211546

Mohamed, R., Fawzy, E., Shehab, R., Ali, D., Salah, R., and Abd, H. (2021). Green biosynthesis, structural characterization and anticancer activity of copper oxide nanoparticles from the brown alga cystoseira myrica. *Egypt. J. Aquat. Biol. Fish.* 25, 341–358. doi: 10.21608/ejabf.2021.189069

Mordechai, S., Mordehai, J., Ramesh, J., Levi, C., Huleihel, M., Erukhimovitch, V., et al. (2001). Application of FTIR microspectroscopy for the follow-up of childhood leukemia chemotherapy. *Proc. SPIE. - Int. Soc. Optical. Eng.* 4491. doi: 10.1117/12.450167

Mosmann, T. (1983). Rapid colorimetric assay for cellular growth and survival: application to proliferation and cytotoxicity assays. *J. Immunol. Methods* 65 (1-2), 55–63. doi: 10.1016/0022-1759(83)90303-4

Murugaboopathy, V., Saravankumar, R., Mangaiyarkarasi, R., Kengadaran, S., Samuel, S. R., and Rajeshkumar, S. (2021). Efficacy of marine algal extracts against oral pathogens - a systematic review. *Indian J. Dent. Res.* 32 (4), 524–527. doi: 10.4103/ijdr.IJDR_243_20

Orłowski, P., Kowalczyk, A., Tomaszewska, E., Ranoszek-Soliwoda, K., Węgrzyn, A., Grzesiak, J., et al. (2018). Antiviral activity of tannic acid modified silver nanoparticles: Potential to activate immune response in herpes genitalis. *Viruses* 10 (10), 2–15. doi: 10.3390/v10100524

Ovais, M., Khalil, A. T., Ayaz, M., Ahmad, I., Nethi, S. K., and Mukherjee, S. (2018). Biosynthesis of metal nanoparticles *via* microbial enzymes: A mechanistic approach. *Int. J. Mol. Sci.* 19 (12), 2–20. doi: 10.3390/ijms19124100

Pinto, R. M., Diez, J. M., and Bosch, A. (1994). Use of the colonic carcinoma cell line CaCo-2 for *In vivo* amplification and detection of enteric viruses. *J. Med. Virol.* 44, 310–315. doi: 10.1002/jmv.1890440317

Rai, M., Ingle, A. P., Gupta, I., and Brandelli, A. (2015). Bioactivity of noble metal nanoparticles decorated with biopolymers and their application in drug delivery. *Int. J. Pharm.* 496 (2), 159–172. doi: 10.1016/j.ijpharm.2015.10.059

Randazzo, W., Piqueras, J., Rodriguez-Diaz, J., Aznar, R., and Sanchez, G. (2018). Improving efficiency of viability-qPCR for selective detection of infectious HAV in food and water samples. *J. Appl. Microbiol.* 124 (4), 958–964. doi: 10.1111/jam.13519

Rauwel, P., Küünal, S., Ferdov, S., and Rauwel, E. (2015). A review on the green synthesis of silver nanoparticles and their morphologies studied *via* TEM. *Adv. Mater. Sci. Eng.* 2015, 1–9. doi: 10.1155/2015/682749

Rayman, M. P. (2012). Selenium and human health. *Lancet* 379 (9822), 1256–1268. doi: 10.1016/s0140-6736(11)61452-9

Razi, M. K., Maamoury, R. S., and Banihashemi, S. (2011). Preparation of nano selenium particles by water solution phase method from industrial dust. *Int. J. Nano. Dimension.* 1 (4), 261–267.

Riyadh, S., Gomha, S., Mahmmoud, E., and Elaasser, M. (2015). ChemInform abstract: Synthesis and anticancer activities of thiazoles, 1,3-thiazines, and thiazolidine using chitosan-Grafted-Poly(vinylpyridine) as basic catalyst. *HETEROCYCLES* 91, 1227. doi: 10.3987/COM-15-13210

Salih, H., Elshehabi, T., and Bilgesu, H. (2016). Impact of nanomaterials on the rheological and filtration properties of water-based drilling fluids. *SPE Eastern Regional Meeting* (Canton, Ohio, USA) pp. SPE-184067-MS. doi: 10.2118/184067-MS

Sharma, B., Purkayastha, D. D., Hazra, S., Gogoi, L., Bhattacharjee, C. R., Ghosh, N. N., et al. (2014). Biosynthesis of gold nanoparticles using a freshwater green alga, prasiola crispa. *Mater. Lett.* 116, 94–97. doi: 10.1016/j.matlet.2013.10.107

Sharma, A., Sharma, S., Sharma, K., Chetri, S. P. K., Vashishtha, A., Singh, P., et al. (2015). Algae as crucial organisms in advancing nanotechnology: a systematic review. *J. Appl. Phycol.* 28 (3), 1759–1774. doi: 10.1007/s10811-015-0715-1

Šileikaitė, A., Puišo, J., Prosyčevas, I., and Tamulevičius, S. (2009). Investigation of silver nanoparticles formation kinetics during reduction of silver nitrate with sodium citrate. *Mater. Sci. (Medžiagotyra).* 15 (1), 21–27.

Silva, S. D., Feliciano, R. P., Boas, L. V., and Bronze, M. R. (2014). Application of FTIR-ATR to moscatel dessert wines for prediction of total phenolic and flavonoid contents and antioxidant capacity. *Food Chem.* 150, 489–493. doi: 10.1016/j.foodchem.2013.11.028

Singh, R. K., Kukrety, A., Sharma, O. P., Baranwal, S., Atray, N., and Ray, S. S. (2016). Study of a novel phenolic-ester as antioxidant additive in lube, biodiesel and blended diesel. *J. Ind. Eng. Chem.* 37, 27–31. doi: 10.1016/j.jiec.2016.03.029

Soliman, M., Saurin, T. A., and Anzanello, M. J. (2018). The impacts of lean production on the complexity of socio-technical systems. *Int. J. Prod. Econ.* 197, 342–357. doi: 10.1016/j.ijpe.2018.01.024

Suganya, K. S. ,. U., Govindaraju, K., Kumar, G., Dhas, S., Velu, K., Singaravelu, G., et al. (2015). Blue green alga mediated synthesis of gold nanoparticles and its antibacterial efficacy against gram positive organisms. *Mater. Sci. Eng.: C.* 47, 351–356. doi: 10.1016/j.msec.2014.11.043

Tahmasebi, P., Javadpour, F., and Sahimi, M. (2015). Three-dimensional stochastic characterization of shale SEM images. *Transport. Porous. Media.* 110 (3), 521–531. doi: 10.1007/s11242-015-0570-1

Thamer, M., Lee, T. C., Wasse, H., Glickman, M. H., Qian, J., Gottlieb, D., et al. (2018). Medicare Costs associated with arteriovenous fistulas among US hemodialysis patients. *Am. J. Kidney Dis.* 72 (1), 10–18. doi: 10.1053/j.ajkd.2018.01.034

Vijayan, P., Raghu, C., Ashok, G., Dhanaraj, S. A., and Suresh, B. (2004). Antiviral activity of medicinal plants of *Nilgiris*. *Indian J. Med. Res.* 120, 24–29.

Vikneshan, M., Saravanakumar, R., Mangaiyarkarasi, R., Rajeshkumar, S., Samuel, S. R., Suganya, M., et al. (2020). Algal biomass as a source for novel oral nano-antimicrobial agent. *Saudi. J. Biol. Sci.* 27 (12), 3753–3758. doi: 10.1016/j.sjbs.2020.08.022

Vincy, W., Mahathalana, T. J., Sukumaran, S., and Jeeva, S. (2017). Algae as a source for synthesis of nanoparticles – a review. *Int. J. Latest. Trends Eng. Technol.*, 005–009.

Xia, L., Chen, D., Su, J., Zheng, R., Ning, Z., Zhao, M., et al. (2022). Selenium nanoparticles inhibited H1N1 influenza virus-induced apoptosis by ROS-mediated signaling pathways. *RSC. Adv.* 12, 3862–3870. doi: 10.1039/D1RA08658H

Younger, P. (2014). *The Merck index. 15th edition* (London: Emerald Group Publishing Limited).

Yue, B., Yang, J., Wang, Y., Huang, C.-Y., Dave, R., and Pfeffer, R. (2004). Particle encapsulation with polymers *via in situ* polymerization in supercritical CO2. *Powder. Technol.* 146 (1-2), 32–45. doi: 10.1016/j.powtec.2004.07.002